applied sciences

MDPI

Article

Impact of Arch Dam Cracking on Monitoring Data

André Conde [1,*], Miguel Á. Toledo [1] and Eduardo Salete [2]

[1] Dam Safety Research Group, Department of Civil Engineering, Hydraulics, Energy and Environment, Universidad Politécnica de Madrid, Profesor Aranguren, s/n, 28040 Madrid, Spain; miguelangel.toledo@upm.es

[2] Escuela Técnica Superior de Ingenieros Industriales, Universidad Nacional de Educación a Distancia, Juan del Rosal 12, 28040 Madrid, Spain; esalete@ind.uned.es

* Correspondence: andre.conde@upm.es

Abstract: It is well established that the proper functioning of dams plays an important role in society. Therefore, as a fundamental part of their safety, the identification of anomalies by monitoring their deformations must be given special consideration. The ability to detect cracks based on monitoring device records depends largely on the number of devices included in the dam's original design, their arrangement, and their accuracy. This paper aims to help determine the appropriate spacing and accuracy of the devices for detecting a given crack. For this purpose, numerical simulations of cracks that match the most likely cracks in arch dams are performed based on a real dam, ensuring that such cracks result in an opening wide enough to be of concern. Afterward, the study analyzes the impact of the length and depth of the crack and the accuracy and position of the monitoring device on the ability of the system to detect the crack.

Keywords: dams; cracks; FEM; monitoring

Academic Editor: Cheng-Yu Ku

Received: 20 December 2024
Revised: 16 January 2025
Accepted: 21 January 2025
Published: 22 January 2025

Citation: Conde, A.; Toledo, M.Á.; Salete, E. Impact of Arch Dam Cracking on Monitoring Data. *Appl. Sci.* **2025**, *15*, 1096. https://doi.org/10.3390/app15031096

1. Introduction

1.1. Cracks in Arch Dams

For centuries, dams have been structures that serve an important role in society, providing water reservoirs, flood control, fresh water supply to the population, and power generation. Unfortunately, the obvious advantages of dams are matched by the risks they pose to downstream populations and properties [1]. According to the report of the American Society of Civil Engineers, there are four categories of risk in dams: (i) high (may cause human losses), (ii) significant (economic losses), (iii) low, and (iv) undetermined. About 17% and 12% of dams belong to the first two categories, respectively [2], which makes it crucial to ensure good structural integrity to protect dams. Norway dams are classified into 5 classes according to the consequences in case of failure, and 12% of the registered dams belong to the two categories with the highest risk [3]. French dams more than 2 m high are classified into three categories, and 24% of them belong to the two categories for which regulations impose a risk assessment study, and the administration inspects class A dams every year and class B dams every 5 years [3]. The safety of a dam and the downstream population depends not only on the quality of its design and construction but also, to a large extent, on adequate maintenance and proper monitoring to control the state of the dam.

Concrete high arch dams are extensively used around the world as the most cost-effective and safest type of dam due to their advantages of high bearing capacity, excellent seismic performance, and high economic efficiency [4–7]. In general, arch dams are at risk

of failure due to structural failure within the dam body, sliding along the dam-foundation interface, or rock settlement under the abutment [8]. However, historically, technicians frequently overlooked identifying the cause of failure for concrete dam rehabilitation, making their decisions based on their experience and intuition [9].

Almost all high arch dams have experienced unexpected cracks, either in the construction phase or during in-service conditions [10–13] due to complex factors such as drying shrinkage, thermal stress, hydraulic thrust, concrete deterioration, or uneven settlement of the dam and foundation. Treating dangerous cracks is of paramount importance, as the development of open cracks decreases the strength and rigidity of the dam, affects its integrity and impermeability, accentuates the deterioration of the concrete, and endangers the safe operation of the dam.

1.2. Monitoring of Arch Dams

The identification of any anomaly is fundamental to the safety assessment of dams. Historically and to this day, the method for measuring ordinary alterations in a dam and detecting potentially dangerous abnormal changes has been performed by employing monitoring devices located in the dam. The first step to understanding how dam monitoring devices identify different types of cracks is to establish the ability of the devices to measure dam deformations. In the early 1970s, the development of automated monitoring systems started for dams, which reduced the tedious work involved in processing and displaying the data. It was not until 1982 that ICOLD first addressed the issue of automated dam monitoring by publishing a comprehensive review of the automation of monitoring systems [14].

It should be noted that monitoring systems (both automatic and manually operated) suffer from accuracy limitations in addition to systematic errors, random errors, and noise [15]. The most commonly monitored parameters in dams are dam body displacement, foundation displacement, water leakage, joint and crack movement, concrete temperature, and external parameters such as stream flow, seismic movement, ice thickness, air temperature and relative humidity, pore pressure, snow and precipitation, water level, and water temperature [16]. As a general rule, concrete dams and hydroelectric power plant structures demand five times more accurate monitoring measurements than embankment dams and slopes enclosing reservoirs [17]. Sensors employed in monitoring measurements are generally divided into geodetic sensing techniques (terrestrial and space) and geotechnical/structural instruments (e.g., pendulum and extensometers). Additional information on the instrumentation used for each of these parameters can be found in [18].

Traditionally, the most precise and widely installed monitoring device to record concrete dam movements has been the pendulum. Pendulum technology has advanced recently, making the monitoring devices installed in some older dams obsolete. From manual sight-reading pendulums, the focus has shifted to devices that employ sensors to automatically measure and continuously send those data to a control center. On the other hand, there is a main branch in geodetic engineering to determine the elevations between two ground points, either directly or indirectly. Geodetic approaches provide data on absolute and relative displacements (changes in coordinates) to derive the displacement and deformation ranges of the monitored structure. Thus, geodetic surveys provide global information on the behavior of the investigated object [17]. These geodetic devices, which traditionally have not been accurate enough to detect deformations less than 1 mm in size [19–23], have improved in the 21st century to the point that it is nowadays possible to employ digital, optical, or laser devices that reach the required accuracy. This work compares various methods and instruments currently used in precise measurements to

assess displacements. Table 1 summarizes the different categories of monitoring devices used in arch dams.

Table 1. Dam monitoring devices for movement measurement.

Device Categories	Minimum Measurement Resolution	Best Offer Accuracy *
Theodolite Electronic distance meter Dumpy level	1 mm	Insufficient: 1 mm
Sighting reading pendulum Digital level Optical level	0.05 mm [24,25]	Low: 0.1 mm [24–27]
Remote reading pendulum station	0.05 mm	Medium: 0.05 mm [17,28,29]
Optical smart pendulum sensor Laser plumbline Laser tracker	0.0001 mm [30]	High: 0.02 mm [18,29,31,32]

* In the case of geodetic devices, accuracy refers to readings from a distance of 160 m.

The type of monitoring devices used in a dam, as well as the number of devices and their position inside the dam, is usually decided based on previous experience in the safety of similar dams, as well as on the budget for the design of the new dam. It is important to consider that the installation of surveillance devices a posteriori inside the dam is not a common practice, as it is usually a complex and costly process. There is a necessity to establish new criteria for the selection and location of dam instrumentation in conformity with the paradigm shift in measurement devices, measurement automation, and evaluation methods. Therefore, this study attempts to shed some light on the implications of the position and type of monitoring devices in an arch dam. For this reason, one of the goals of this work is to help determine the required distance and accuracy of the monitoring devices destined to detect cracks.

1.3. Numerical Background

Numerical models have proven to be important tools for the study and validation of hypotheses developed during the diagnostic procedure of the different pathologies that affect concrete dams [33–35]. In particular, the finite element method (FEM) [36], as the most commonly used numerical method, has been widely used to solve contact problems. It is important to note that the different options for modeling structures in simulation packages are not usually equivalent, so different finite element method programs implement different mathematical models to solve cracks or contraction joints. There are several studies on cracked arch dam calculations showing the location of the crack (most of them involving nonlinear finite elements where each element can transition to a cracked state) as a result of deformations and certain formulations [37–41]. Similarly, many arch dam computational studies incorporate contraction joints between cantilevers, with each cantilever of the dam behaving in a linear elastic way. However, the dam exhibits nonlinear behavior, and therefore the inclusion of a nonlinear component at the interface between the cantilevered faces in contact is recommended [42,43]. The reason for this is the presence of contraction joints that may open under frictional forces. To avoid these complexities of nonlinear solutions, this study employs an accurate dam-solving methodology that has been previously described and validated [44]. For a better understanding of this method, a summary can be found in Section 2.1.

2. Methods

2.1. Numerical Approach

A campaign of FEM simulations was conducted on a real dam to which different cracks of variable lengths, depths, positions, and orientations were applied. It was determined which records would be obtained by monitoring devices at different points of the dam to analyze whether they were able to detect cracks as a function of the accuracy and position of the device. The Ansys Mechanical Finite Element Analysis Software for Structural Engineering 2022 [45], in combination with 3D designs, was used to perform all these numerical simulations of the dam–soil system contemplated in this work. The model used had the following features: (a) linear materials (stress–strain curve); (b) static models; (c) no separation between the dam and the ground; (d) structural loads; (e) nonlinear contacts (cracks).

The complexity of nonlinear materials has not been considered in this study to achieve more time-efficient performance of the simulations. Furthermore, the consideration of linear models generally leads to smaller displacements. Given that the objective of the work carried out is to search for the possibility of detecting cracks from the recorded displacements, the choice of linear models to obtain said displacements will offer more conservative results. Additionally, thermal loads have not been included, as the consideration of temperature would introduce an unnecessary element of complexity, since the goal of the study aims to assess the impact on the monitoring of cracks in different locations and severity, regardless of their cause. Therefore, the self-weight of the dam and the hydrostatic pressure of the reservoir on the upstream face of the dam are the only active forces. Hydrostatic pressure inside the crack is considered because it significantly affects the results (as shown in Section 2.2.4); the pressure is included by applying to both inner faces of the crack the same mathematical modeling as to the submerged faces of the upstream face. For this purpose, the hydrostatic pressure is considered to remain inside the crack as a function of elevation.

The methodology adopted for numerical modeling addresses the fact that the structure of the dam changes due to self-weight before contraction joint sealing and hydrostatic pressure development. The contraction joint grouting transforms the individual cantilevers into a monolithic body. Such a configuration of the dam changes again as soon as a crack opens up.

The boundary conditions for the simulated models were typical for this type of model and consisted of restricting horizontal movements on the sides of the soil body and restricting any movement at the lower base of the soil. As it was a static analysis, pure displacement constraints were considered. The dimensions of the 3D model on each side of the structure were enough for the boundary conditions applied not to affect the results: vertically, a minimum depth of soil of 150% of the height of the dam was considered, while the lateral expansion was at least 50% of the length of the dam without abutments.

2.2. Case Study

In this article, a concrete arch dam is analyzed. It is the La Baells dam, on the Llobregat River, located in the province of Barcelona (Spain). The reservoir has a capacity of 109.5 hm^3. This dam was built in 1976 with a height of 102.3 m and a crest length of 302.4 m.

The physical properties of the materials (bedrock and concrete) were established following the findings of previous studies carried out in La Baells [44] (Table 2). The bedrock is formed by a multitude of narrow and almost vertical strata, allowing for a simplification to average values of the rock properties; therefore, it is considered that the foundation materials are homogeneous. Following the reports of the Concrete Masonry

Handbook [46] and the PCI Design Handbook [47], a concrete-to-concrete coefficient of friction for dry conditions of 0.8 is adopted.

Table 2. Properties of materials.

Material	Foundation	Concrete
Density (kg/m^3)	3000	2400
Modulus of elasticity (MPa)	42,831.87	31,877.02
Poisson's ratio	0.25	0.22

Thermal stresses are not relevant for the purpose of this research and were omitted in part to additionally achieve a manageable computational time, as were seismic stresses, chemical effects, and constructional failures. It became necessary to consider cracks that would open wide enough to modify the dam response; however, dams are designed to operate under the expected loading conditions without developing significant cracks. Therefore, to open cracks that would open significantly in the dam studied under hydraulic loads alone, it was required to impose extraordinary loads. The reservoir level for the base simulations studied was set at 645 m above sea level, which corresponds to an unrealistic overtopping of 17 m. However, the loads do not affect the objective of the paper, which is to analyze the effect of open cracks on monitoring. It should be noted that the aim of the analysis is not to obtain a realistic stress distribution but to be able to analyze at which point a monitoring device may or may not detect a crack in the dam. The virtual hydraulic load instead of an imposed deformation has the advantage that it would produce more realistic movements within the body of the dam.

2.2.1. Geometrical Characterization

The 3D geometrical model was elaborated based on the topographical reports and the available design sections of the dam (the tallest section can be seen in Figure 1). However, only the soil close to the dam is mapped by adjusting the contour lines (every five meters), while the soil not adjacent to the dam has been simplified to achieve a more efficient mesh and faster calculations (Figure 2).

The dam has 17 contraction joints (the ones on the right side are shown in Figure 2) which, when open, allow the cantilevers to slide independently of each other. The applied mesh is composed of 10-node tetrahedra according to the parameters set out in [44] to maintain a compromise between the calculation time and the quality of the result. Finally, the main parameters of the mesh are (a) quadratic order of the elements; (b) growth ratio of 1.1; (c) maximum mesh size of 1.15 m for the dam and 11.5 m for the bedrock; (d) around 1.2 million elements; (e) around 1.8 million nodes.

2.2.2. Cracks

For the analysis of the cracking effect, it was assumed that a fully developed significant crack existed in the dam. The mesh is then projected by aligning the faces of the elements with the sides of the crack. The crack was considered to be fully formed, thus not taking into account the development process. The crack faces perform according to their real behavior: they can transmit compressive and frictional forces, and they can move independently if they do not intersect each other.

To provide a more general analysis, a set of 14 cracks of the most common shape and location for arch dams was simulated [48] (to avoid restricting the study to only the most likely cracks for the particular geometry of the 3D design). The set was completed, symmetrically, with the addition of two more cracks (denominated 4.1U and 4.2U), although these two additional cracks would only appear due to specific design or construction

failures. The cracks were simulated independently; they never coexisted in the same model in order to generate more understandable information.

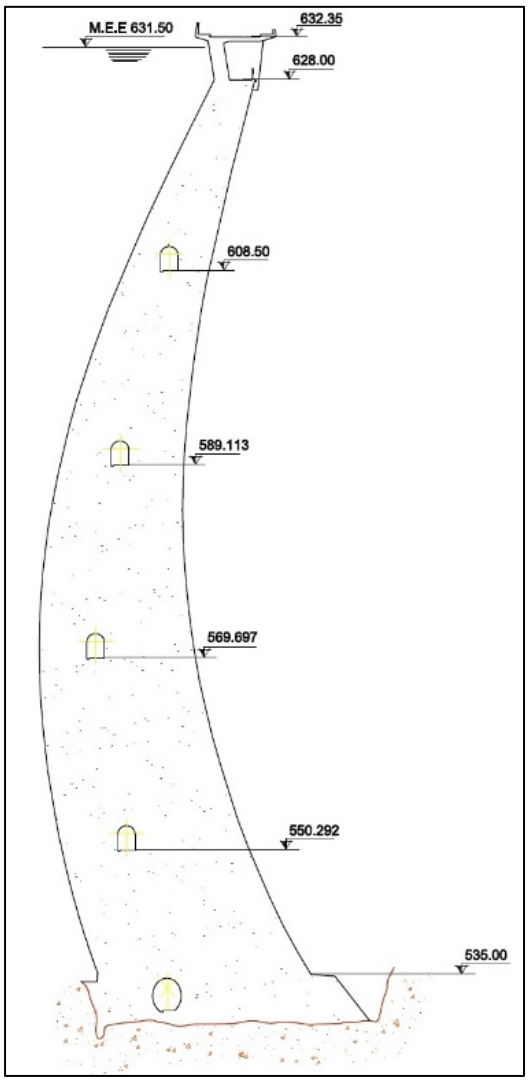

Figure 1. Cross-section of La Baells dam.

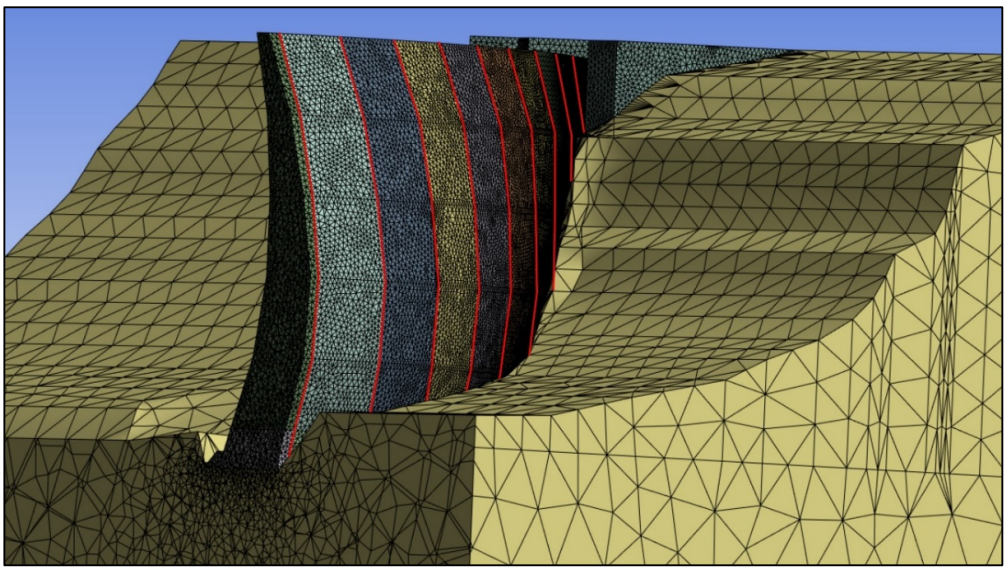

Figure 2. Mesh of half dam and foundation showing the locations of contraction joints (red lines).

Different lengths and depths of certain significance were considered for the cracks. Initially, the maximum depth of each crack varies between 2 and 3.3 m, although the depth was doubled at a later stage to study the effect of depth on the results. The locations of the cracks are shown in Figure 3, while other details of the cracks are shown in Table 3.

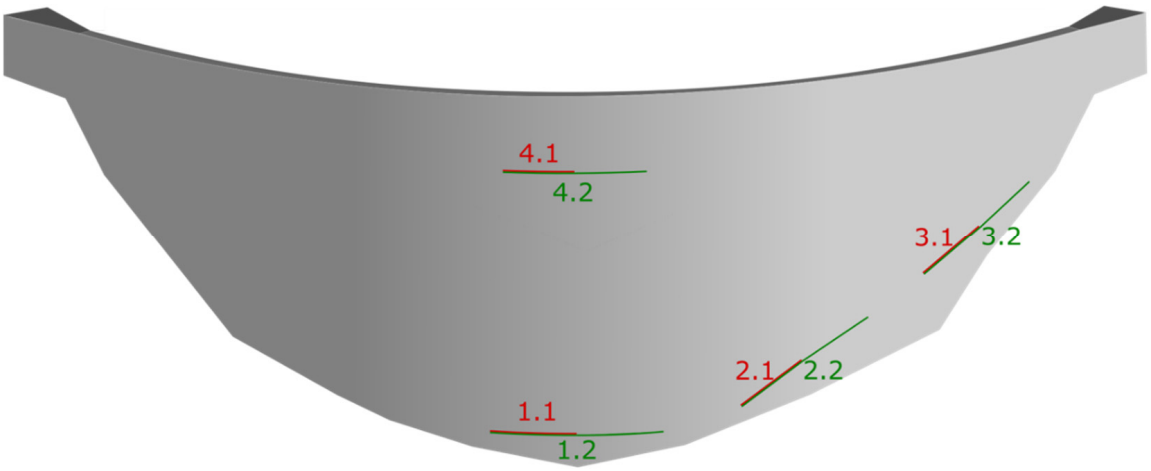

Figure 3. Upstream cracks (#.1 for length one cantilever, #.2 for length two cantilevers). Downstream cracks are located in analogous positions.

Table 3. Crack characteristics.

Name	Length	Mean Height Above the Base of the Dam	Face	Orientation
1.1U	22.9 m	9.5 m	Upstream	Horizontal
1.1D	20.0 m	9.5 m	Downstream	Horizontal
1.2U	45.4 m	9.5 m	Upstream	Horizontal
1.2D	38.9 m	9.5 m	Downstream	Horizontal
2.1U	19.7 m	25.5 m	Upstream	Oblique
2.1D	17.9 m	25.5 m	Downstream	Oblique
2.2U	41.6 m	25.5 m	Upstream	Oblique
2.2D	37.2 m	25.5 m	Downstream	Oblique
3.1U	20.3 m	52.5 m	Upstream	Oblique
3.1D	18.9 m	52.5 m	Downstream	Oblique
3.2U	42.5 m	52.5 m	Upstream	Oblique
3.2D	38.6 m	52.5 m	Downstream	Oblique
4.1U	18.8 m	79.5 m	Upstream	Horizontal
4.1D	17.7 m	79.5 m	Downstream	Horizontal
4.2U	37.5 m	79.5 m	Upstream	Horizontal
4.2D	35.4 m	79.5 m	Downstream	Horizontal

2.2.3. Pressure Inside the Crack

The necessity of applying internal pressure has been comparatively analyzed for the largest horizontal crack upstream and the largest diagonal crack upstream, exploring the effect of considering the hydrostatic pressure on the internal faces of the crack in the increase in displacements measured on all the monitoring devices (Figure 4). It can be seen in the data that the average error reaches 42% when the increments are more than 0.1 mm., and it stands at 78% if they are lower than 0.1 mm.

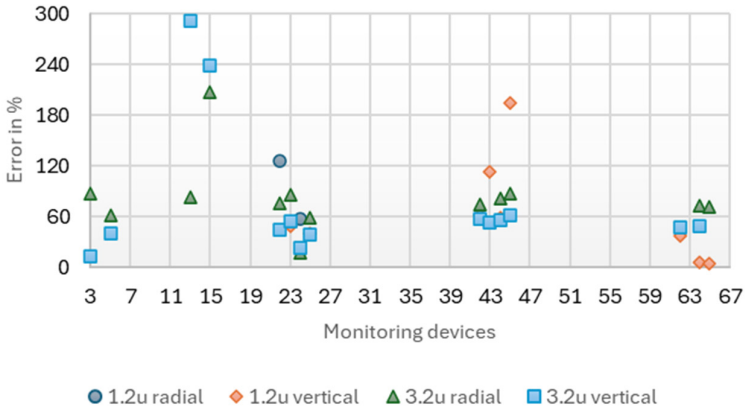

Figure 4. Error in displacement increments due to disregarding the internal pressure in the crack.

2.2.4. Monitoring Devices

A broad set of virtual auscultation points was implemented for the analysis of the importance of the position of monitoring devices in the dam. Some of these virtual devices correspond to actual devices located near the center and on the left side of the dam (devices 1D-P0, 2I-P0, and 6I-P0), as well as devices located at half the height on the same cantilevers (devices 1D-P2, 2I-P2, and 6I-P2). In addition, extra monitoring points were placed which cannot be monitored in the real dam, simulating a more complete monitoring system (Figure 5). The additional monitoring points are located on the crest of each cantilever (to represent geodetic devices) and in the interior of each cantilever, following the same pattern as the real pendulums. Since the behavior of the dam is relatively symmetrical, only one half of the dam has been placed with additional monitoring points.

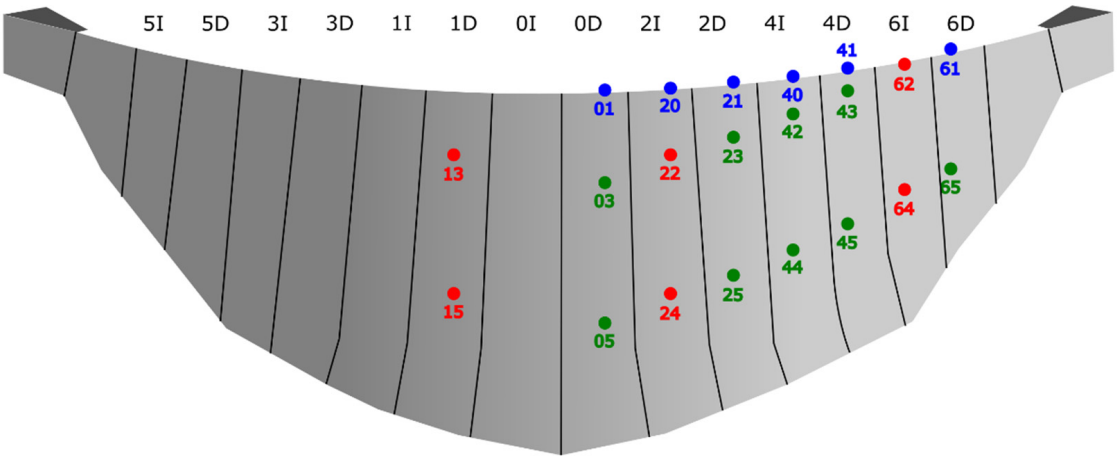

Figure 5. Identification numbers for virtual monitoring devices for dam displacement measurement (first digit points to the cantilever identification). Red: location of actual devices; green: additional internal devices; blue: additional devices on the crest.

3. Results

The results obtained for each of the considered cracks are presented below.

3.1. Crack 1

For the upstream crack position, the openings resulted in 1.48 mm (1.1U) and 1.53 mm (1.2U). It can be observed that the maximum increment of radial displacement due to the crack is 0.4 mm (Figure 6). It is not intuitive that displacement in devices 40 and 42 is higher for the shorter crack than for the longer one. The reason for this is that, in the cantilevers closer to the center of the dam, the displacement increases occur downstream, while near

the abutment, the displacement increases are in the upstream direction. Doubling the crack length shifts the point where the increments change direction from cantilever 2D to 4I, and thus the increments change from the downstream direction to the upstream direction at points 40 and 42. On the other hand, the downstream crack position does not open and produces changes generally below 0.005 mm.

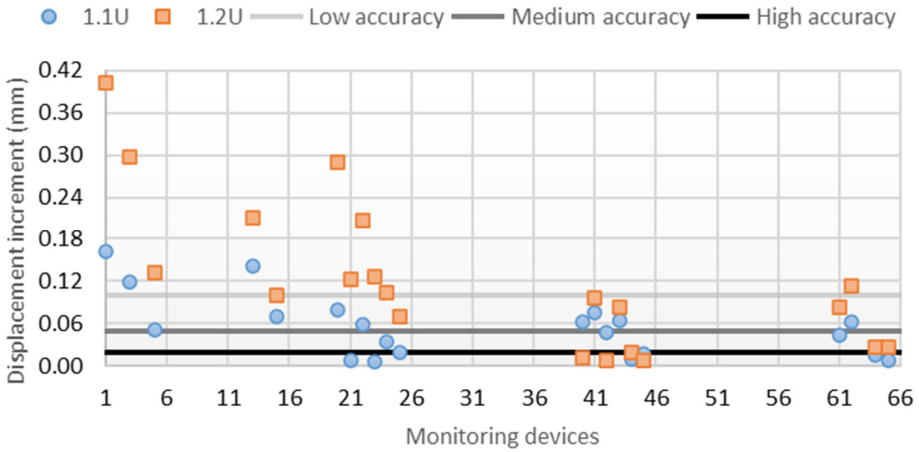

Figure 6. Absolute increase in radial displacement at the crest level due to crack 1. Low, medium, and high accuracy of monitoring devices are included for comparison.

Furthermore, cracks twice as deep were analyzed to compare the deformations (Table A1 of the Appendix A). Doubling the depth of the crack increases the crack opening by around 74%. All simulated values for the movements at the locations of the virtual monitoring devices resulting from each of the type 1 cracks can be found in Table A5 of the Appendix A.

3.2. Crack 2

For this crack, at the upstream face position, the maximum crack opening is 0.85 mm. It is worth noting that there is no change in the maximum opening between 2.1U and 2.2U. As can be seen in the results, the maximum increment in radial displacement is 0.27 mm (Figure 7). In contrast to crack 1, crack 2 produces an increase in displacement of up to 0.05 mm while still being closed.

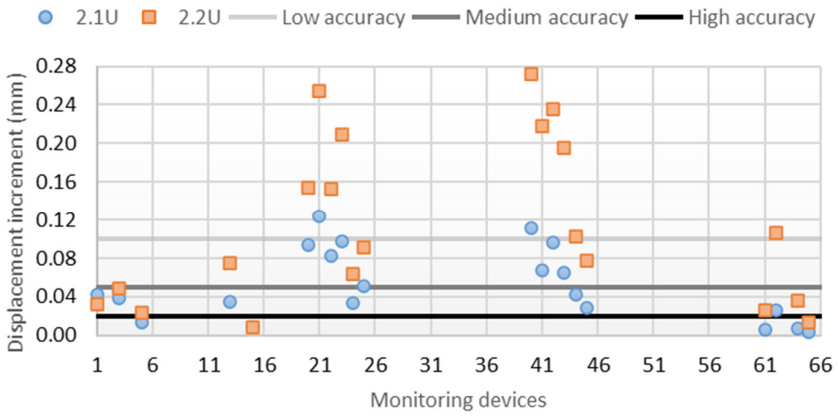

Figure 7. Absolute increase in radial displacement at the crest level due to crack 2. Low, medium, and high accuracy of monitoring devices are included for comparison.

It should be noted that, although the downstream cracks do not open, they do affect the recorded deformations in the same order of magnitude as the upstream cracks. The reason for this may be that one side of the crack slides relative to the other not only in the

radial direction but also in the vertical direction. The same effect can be seen in the analysis of crack 3 in the following section.

Furthermore, cracks twice as deep were analyzed to compare deformations (Table A2 of the Appendix A). Again, the previously reported result for the type 1 crack that double depth significantly impacts crack opening is observed; a 73% increase was observed for the type 2 crack. All simulated values for the movements at the locations of the virtual monitoring devices resulting from each of the type 2 cracks can be found in Table A6 of the Appendix A.

3.3. Crack 3

The crack 3 maximum openings for the crack on the upstream face are 0.62 mm (3.1U) and 0.71 mm (3.2U), and the maximum radial displacement increment due to the crack is 0.37 mm. Increases in radial displacements due to the cracks on the upstream face are shown in Figure 8. The increase in displacement with these type 3 cracks located on the upstream face, which remain closed, reaches a value up to 0.02 mm, lower than that corresponding to type 2 cracks (0.05 mm), but significantly higher than that obtained for type 1 cracks (less than 0.005 mm).

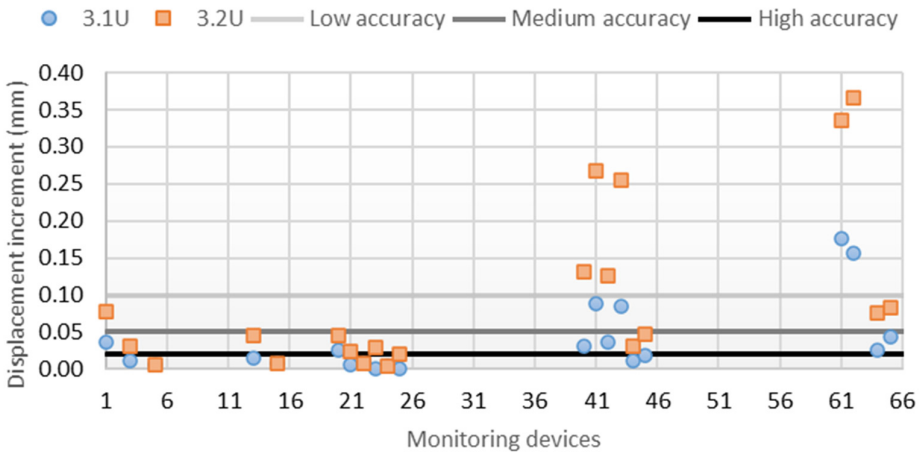

Figure 8. Absolute increase in radial displacement at the crest level due to crack 3. Low, medium, and high accuracy of monitoring devices are included for comparison.

For these type 3 cracks, twice-deeper cracks were also analyzed to compare deformations (Table A3 of the Appendix A). Again, the previously reported result for type 1 and type 2 cracks that double-depth significantly impacts crack opening is observed: there was a 76% increase for the type 3 crack.

All simulated values for the movements at the locations of the virtual monitoring devices resulting from each of the type 3 cracks can be found in Table A7 of the Appendix A.

3.4. Crack 4

Crack 4 is located in the upper part of the dam, in the central cantilever. The simulated depths of this crack are shown in Table A4 of the Appendix A. The depths of the cracks were not doubled, as this would mean a crack that exceeds half the thickness of the dam, something that would be extremely unusual in reality. Table A8 of the Appendix A shows the movements observed on the virtual monitoring devices that would produce each of the cracks.

It should be noted that no type 4 crack opens up; this effect is assumed to occur because the hydraulic load creates tension just in the upstream areas of the dam close to the ground. It can be found that all displacement increments due to cracks are less than 0.005 mm.

4. Discussion

An analysis was conducted to evaluate the effects of doubling the crack length on changes in recordings (Figure 9). Displacement increments below 0.01 mm were excluded to prevent distortion from relative comparisons of small values. After removing outliers, the average multiplication factor for doubling crack length was 2.34. A trend shift was observed as displacement transitioned from upstream to downstream, at values of 65 m (crack 1), −65 m (crack 2), and −75 m (crack 3).

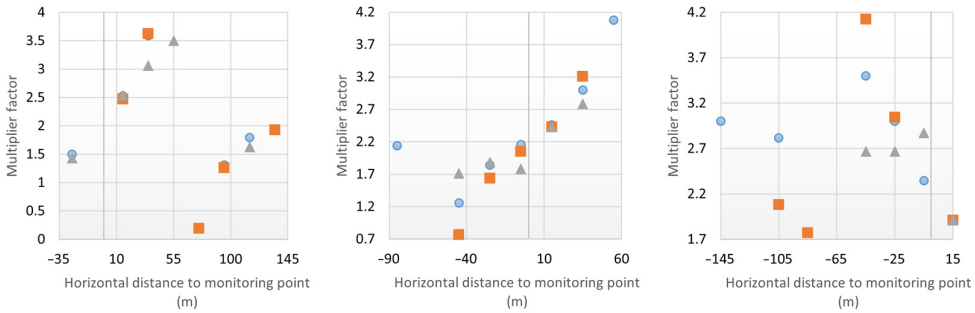

Figure 9. Effect of doubling the length on displacements in crack 1 (**left**), crack 2 (**center**), and crack 3 (**right**). Orange square: coronation. Blue circle: medium height. Gray triangle: lower height. Vertical gray line: monitoring point.

Figures 10 and 11 examine the effect of doubling crack depth on changes in recorded displacements. Displacement increments below 0.01 mm were excluded. Excluding outliers, the average multiplication factor for doubling crack depth was 2.6.

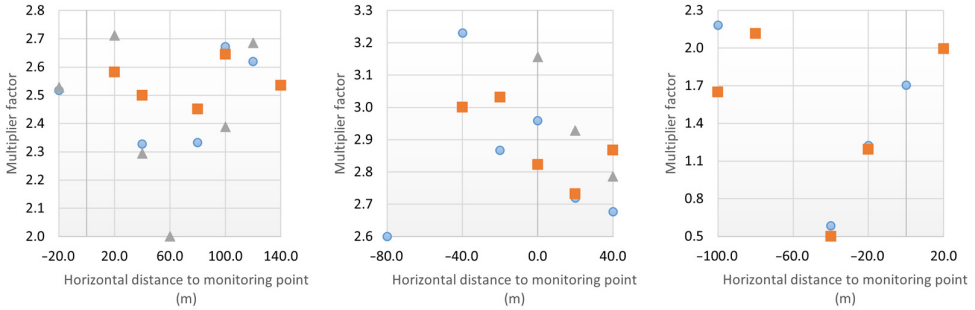

Figure 10. Effect of doubling the depth on the displacements (length of one cantilever) in crack 1 (**left**), crack 2 (**center**), and crack 3 (**right**). Orange square: coronation. Blue circle: medium height. Gray triangle: lower height. Vertical gray line: monitoring point.

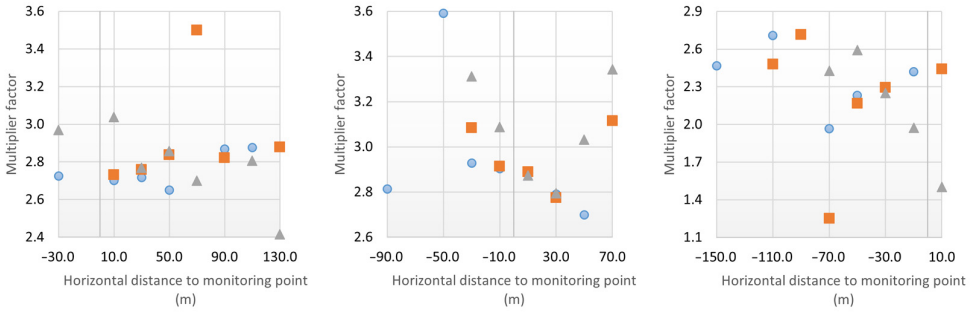

Figure 11. Effect of doubling the depth on the displacements (length of two cantilevers) in crack 1 (**left**), crack 2 (**center**), and crack 3 (**right**). Orange square: coronation. Blue circle: medium height. Gray triangle: lower height. Vertical gray line: monitoring point.

Figure 12 analyzes the displacement increments of upstream crack 1 under varying simulation parameters. It uses the configuration causing the largest displacements (crack

1.2U*) as a reference. Displacement increments for halving crack depth, halving crack length, and reducing the reservoir level by 20 m are compared across monitoring devices. It is determined that reducing the reservoir level by 20 m yields similar results to the reduction in crack depth or length. While reductions in crack depth and reservoir level produce comparable displacements and crack openings, halving crack length results in a similar average displacement reduction but with a distinct distribution and significantly different crack openings.

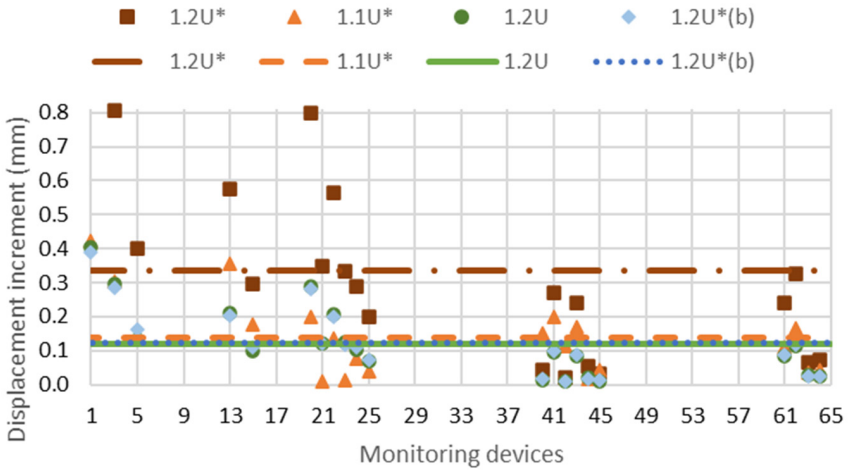

Figure 12. Increases in radial displacements (and mean values) due to different configurations of crack 1.

Figure 13 compares the impact of reservoir level reduction on displacements recorded by monitoring devices for case 1.2U* (see Table A9 in the Appendix A). The average multiplication factors are 1.61 (12 m), 2.06 (16 m), 2.74 (20 m), and 3.26 (22 m). The results indicate a relationship ranging from 6.8 to 7.8 between reservoir level variation and the increment multiplication factor variation.

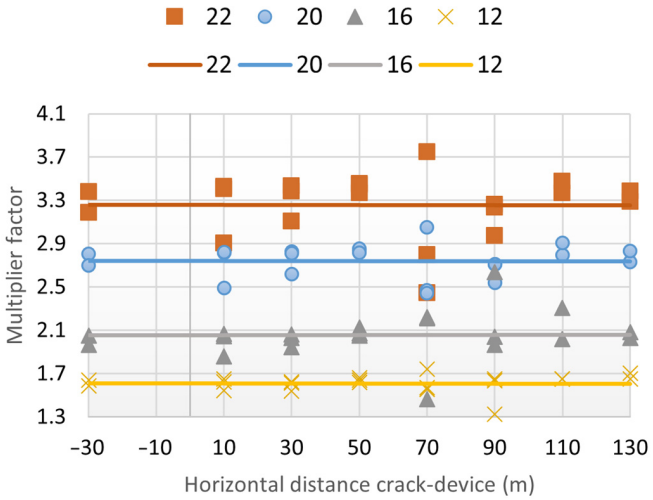

Figure 13. Effect of increasing the reservoir level on displacements (and mean values).

A comparison is made between cracks with similar maximum openings (within a 4% tolerance), selected from each position (excluding position 4, where cracks do not open), and differing parameters. Numerical results are provided in Table A10 (Appendix A). Figures 14–16 present displacement data recorded by monitoring devices as a function of horizontal distance from the crack center, excluding crest records due to significant vertical

distance variations. Cracks with similar openings exhibit comparable effects on monitoring device recordings.

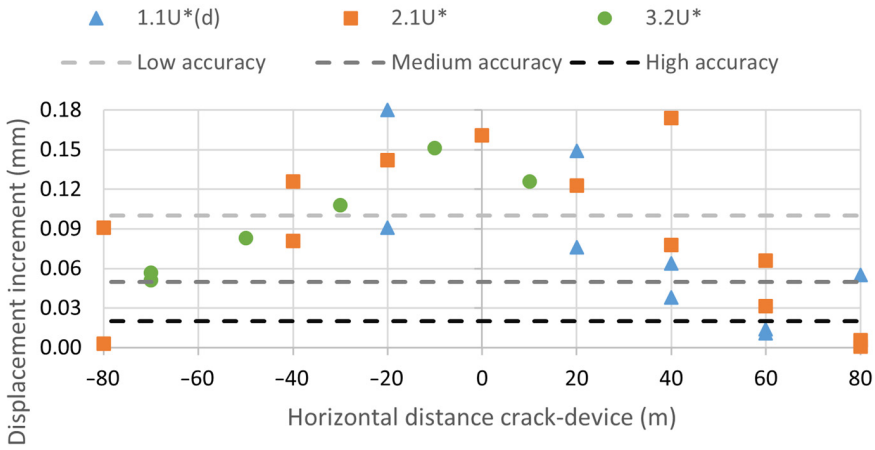

Figure 14. Comparison of different cracks causing 1.25 mm opening. Horizontal distance is rounded to 5 m intervals. The reservoir level for 1.1U*(d) is 629.2 m above sea level.

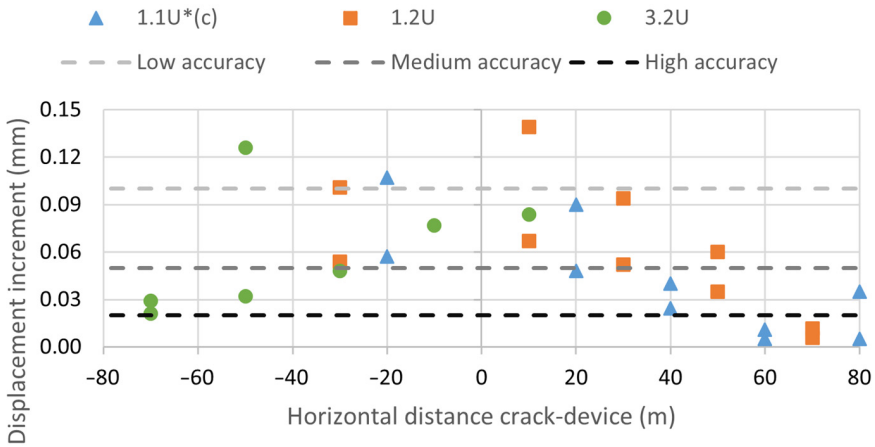

Figure 15. Comparison of different cracks causing 0.73 mm opening. Horizontal distance is rounded to 5 m intervals. Reservoir level for 1.1U*(c) is 623 m above sea level.

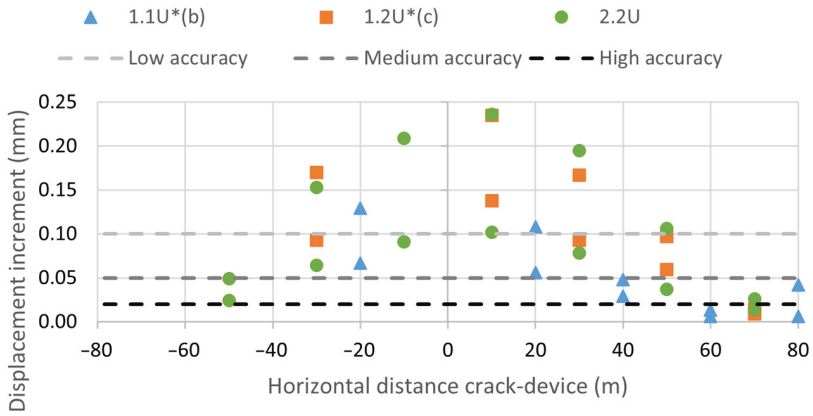

Figure 16. Comparison of different cracks causing 0.88 mm opening. Horizontal distance is rounded to 5 m intervals. Reservoir level for 1.1U*(b) is 625 m above sea level and for 1.2U*(c) is 623 m above sea level.

These figures demonstrate that the horizontal distance between the crack and the measurement point significantly affects crack detection. The difference between whether

the measuring point is 20 m or 40 m horizontally away may determine detection capability. Regarding monitoring device precision:

- A low-accuracy device detects cracks that open more than 0.8 mm if within 20 m horizontally of the crack center.
- A medium-accuracy device detects cracks that open more than 0.8 mm if within 40 m.
- A high-accuracy device detects cracks that open more than 0.8 mm if within 70 m.

5. Conclusions

A total of 35 different cases were simulated with a finite element model of an arch dam based on 28 different cracks. It was determined how they affect the displacement recordings at 15 internal monitoring devices and 6 measurement points at the crest. Twelve of the cracks studied have opened, and a detailed analysis of these cracks leads to significant conclusions, supported by concrete data:

Precision of Monitoring Devices: The precision of monitoring devices is crucial for effectively detecting cracks. Optical smart sensors and laser plumb lines, with precision up to 0.02 mm, are essential for capturing subtle displacements that indicate crack presence. A monitoring device with an accuracy of 0.05 mm can detect a crack horizontally away (40 m in the study) from the center of the crack if the maximum opening is relevant (at least 0.8 mm in the study).

Influence of Crack Length and Depth: Data indicate that doubling the depth of the crack substantially amplifies the opening (by about 75% in the study) and largely amplifies the increments in the records of monitored devices (by about 160% in the study). At the same time, doubling the crack length amplifies in a comparable ratio the increments in records of monitored devices (multiplied by 2.35 in the study).

Influence of Reservoir Level: Given a crack of considerable length (45.4 m in the study) and a depth of 30% of the dam thickness located in the most likely crack zone, increasing the reservoir by X meters multiplies the increases in displacements by a value an order of magnitude lower (close to X/7.3 in the study).

Location of Cracks: Cracks in different locations exhibit distinct displacement patterns. Upstream cracks generate larger radial increments in displacements, whereas those downstream may not open under normal loads but still affect measurements due to relative vertical and radial sliding.

Internal Hydrostatic Pressure: Ignoring hydrostatic pressure inside cracks leads to significant errors (averaging 42% when increments exceed 0.1 mm and up to 78% if they are smaller).

Monitoring System Configuration: The arrangement and number of devices directly influence the ability to detect cracks. A well-distributed and dense system significantly enhances the detection of structural anomalies. The study employed additional virtual devices to simulate a more comprehensive system, located at mid-height and crest levels. It is not straightforward to identify the position of the crack directly from the monitoring results. The fact that the measurement point is 20 or 40 m horizontally distant from the center of the crack can be decisive for the detection of the crack.

Relationship Between the Position of the Crack and the Position of the Monitoring Device: The alterations produced by crack A in the results recorded by device A are similar to the alterations produced by crack B in the results recorded by device B if both cracks have the same opening and the devices are located at the same distance from their crack.

In summary, the most effective devices for detecting cracks, as shown in Table 1, can detect significant cracks located near the foundation (in the studied dam, that means openings greater than 0.62 mm and radial displacement increments over 0.27 mm). These findings underscore the critical importance of meticulous monitoring system design to

ensure the continuous structural safety and operational integrity of arch dams. This study also serves as a basis for future lines of research, such as further developing the analysis of Figure 13 to determine which monitoring strategies are most appropriate depending on the expected reservoir levels.

Author Contributions: Conceptualization, M.Á.T.; methodology, M.Á.T., A.C. and E.S.; validation, A.C.; investigation, A.C.; writing—original draft preparation, A.C.; writing—review and editing, M.Á.T. and E.S.; supervision, M.Á.T. and E.S.; project administration, M.Á.T.; funding acquisition, M.Á.T. All authors have read and agreed to the published version of the manuscript.

Funding: This research was funded by the Spanish Ministry of Science and Innovation within the CORCHEA Research Project (grant number PID2020-118820RB-I00).

Institutional Review Board Statement: Not applicable.

Informed Consent Statement: Not applicable.

Data Availability Statement: The raw data supporting the conclusions of this article will be made available by the authors on request.

Acknowledgments: We are grateful to the research group SERPA-Dam Safety Research, the company ACIS2in, and Agencia Catalana de l'Aigua for the support provided.

Conflicts of Interest: The authors declare no conflicts of interest.

Appendix A

Tables A1–A4 show absolute and relative depths of cracks related to the thickness of the dam.

Table A1. Absolute and relative depths of crack 1 related to the thickness of the dam.

Crack	Maximum Depth		Deeper Crack	Maximum Depth	
	Total	Relative		Total	Relative
1.1U	3.3 m	17%	1.1U*	5.8 m	30%
1.1D	2.4 m	12%	1.1D*	4.8 m	25%
1.2U	3.3 m	17%	1.2U*	5.8 m	30%
1.2D	2.4 m	12%	1.2D*	4.8 m	25%

Table A2. Absolute and relative depths of crack 2 related to the thickness of the dam.

Crack	Maximum Depth		Deep Crack	Maximum Depth	
	Total	Relative		Total	Relative
2.1U	2.8 m	13%	2.1U*	5.5 m	25%
2.1D	3.1 m	14%	2.1D*	5.8 m	26%
2.2U	2.8 m	13%	2.2U*	5.5 m	25%
2.2D	3.1 m	14%	2.2D*	5.8 m	26%

Table A3. Absolute and relative depths of crack 3 related to the thickness of the dam.

Crack	Maximum Depth		Deep Crack	Maximum Depth	
	Total	Relative		Total	Relative
3.1U	2.3 m	14%	3.1U*	4.6 m	27%
3.1D	2.3 m	14%	3.1D*	4.6 m	27%
3.2U	2.4 m	14%	3.2U*	4.8 m	28%
3.2D	2.4 m	14%	3.2D*	4.8 m	28%

Table A4. Depths for crack 3 (relative depths in relation to the thickness of the dam).

Crack	Maximum Depth	
	Total	Relative
4.1U	2.4 m	33%
4.1D	2.0 m	27%
4.2U	2.4 m	33%
4.2D	2.0 m	27%

Tables A5–A9 show, in their first column, the simulated movements that would be recorded by the monitoring devices in the case without a crack. The remaining columns present the increments in displacement (in absolute value) that would be produced by each of the cracks.

Table A5. Crack1. Radial displacements in mm.

	No Crack	1.1U	1.2U	1.1U*	1.2U*
Opening	0.00	1.48	1.53	2.46	2.80
01: 0D crest	−41.33	−0.16	−0.40	−0.42	−1.10
03: 0D-P0	−33.45	−0.12	−0.30	−0.31	−0.81
05: 0D-P2	−15.84	−0.05	−0.13	−0.14	−0.40
13: 1D-P0	−34.12	−0.14	−0.21	−0.35	−0.58
15: 1D-P2	−15.96	−0.07	−0.10	−0.18	−0.30
20: 2I crest	−41.79	−0.08	−0.29	−0.20	−0.80
22: 2I-P0	−34.40	−0.06	−0.21	−0.13	−0.56
24: 2I-P2	−16.10	−0.03	−0.10	−0.08	−0.29
21: 2D crest	−42.26	0.01	−0.12	0.01	−0.35
23: 2D-P0	−35.60	−0.01	−0.13	−0.01	−0.33
25: 2D-P2	−16.25	−0.02	−0.07	−0.04	−0.20
40: 4I crest	−40.97	0.06	0.01	0.15	0.04
42: 4I-P0	−35.10	0.05	0.01	0.11	0.02
44: 4I-P2	−14.32	0.01	−0.02	0.02	−0.05
41: 4D crest	−35.19	0.08	0.10	0.20	0.27
43: 4D-P0	−31.84	0.06	0.08	0.17	0.24
45: 4D-P2	−11.86	0.02	0.01	0.04	0.03
62: 6I-P0	−25.41	0.06	0.11	0.16	0.32
64: 6I-P2	−8.49	0.02	0.03	0.04	0.07
61: 6D crest	−16.45	0.04	0.08	0.11	0.24
65: 6D-P2	−5.43	0.01	0.03	0.04	0.07

Table A6. Crack 2. Radial displacements in mm.

	No Crack	2.1U	2.2U	2.1U*	2.2U*
Opening	0.00	0.85	0.85	1.29	1.66
01: 0D crest	−41.33	−0.04	−0.03	−0.13	−0.14
03: 0D-P0	−33.45	−0.04	−0.05	−0.13	−0.18
05: 0D-P2	−15.84	−0.01	−0.02	−0.08	−0.11
13: 1D-P0	−34.12	0.04	0.08	0.09	0.21
15: 1D-P2	−15.96	0.01	0.01	0.00	0.03
20: 2I crest	−41.79	−0.09	−0.15	−0.28	−0.48
22: 2I-P0	−34.40	−0.08	−0.15	−0.24	−0.45
24: 2I-P2	−16.10	−0.03	−0.06	−0.14	−0.21
21: 2D crest	−42.26	−0.12	−0.25	−0.35	−0.74
23: 2D-P0	−35.60	−0.10	−0.21	−0.29	−0.61
25: 2D-P2	−16.25	−0.05	−0.09	−0.16	−0.28

Table A6. *Cont.*

	No Crack	2.1U	2.2U	2.1U*	2.2U*
40: 4I crest	−40.97	−0.11	−0.27	−0.31	−0.79
42: 4I-P0	−35.10	−0.10	−0.24	−0.26	−0.68
44: 4I-P2	−14.32	−0.04	−0.10	−0.12	−0.29
41: 4D crest	−35.19	−0.07	−0.22	−0.20	−0.61
43: 4D-P0	−31.84	−0.07	−0.20	−0.17	−0.54
45: 4D-P2	−11.86	−0.03	−0.08	−0.08	−0.22
62: 6I-P0	−25.41	−0.03	−0.11	−0.07	−0.29
64: 6I-P2	−8.49	−0.01	−0.04	−0.03	−0.11
61: 6D crest	−16.45	−0.01	−0.03	0.00	−0.08
65: 6D-P2	−5.43	0.00	−0.01	−0.01	−0.05

Table A7. Crack 3. Radial displacements in mm.

	No Crack	3.1U	3.2U	3.1U*	3.2U*
Opening	0.00	0.62	0.71	1.00	1.29
01: 0D crest	−41.33	0.04	0.08	0.06	0.19
03: 0D-P0	−33.45	0.01	0.03	0.02	0.08
05: 0D-P2	−15.84	0.01	0.01	−0.01	−0.02
13: 1D-P0	−34.12	0.02	0.05	0.02	0.11
15: 1D-P2	−15.96	0.01	0.01	0.00	0.01
20: 2I crest	−41.79	0.03	0.05	0.05	0.13
22: 2I-P0	−34.40	0.01	0.01	0.02	0.02
24: 2I-P2	−16.10	0.00	0.00	−0.01	−0.03
21: 2D crest	−42.26	0.01	−0.02	0.04	−0.03
23: 2D-P0	−35.60	0.00	−0.03	0.02	−0.06
25: 2D-P2	−16.25	0.00	−0.02	−0.01	−0.05
40: 4I crest	−40.97	−0.03	−0.13	−0.02	−0.29
42: 4I-P0	−35.10	−0.04	−0.13	−0.02	−0.28
44: 4I-P2	−14.32	−0.01	−0.03	0.00	−0.08
41: 4D crest	−35.19	−0.09	−0.27	−0.11	−0.62
43: 4D-P0	−31.84	−0.09	−0.26	−0.10	−0.58
45: 4D-P2	−11.86	−0.02	−0.05	−0.01	−0.11
62: 6I-P0	−25.41	−0.16	−0.37	−0.27	−0.89
64: 6I-P2	−8.49	−0.03	−0.08	0.01	−0.15
61: 6D crest	−16.45	−0.18	−0.34	−0.35	−0.82
65: 6D-P2	−5.43	−0.04	−0.08	0.00	−0.13

Table A8. Crack 4. Displacements in mm on the real monitoring devices.

	No Crack	4.1U	4.2U
Opening	0.00	0.00	0.00
13: 1D-P0	−34.12	0.00	0.00
15: 1D-P2	−15.96	0.00	0.00
22: 2I-P0	−34.40	0.00	0.01
24: 2I-P2	−16.10	0.00	0.00
62: 6I-P0	−25.41	0.00	0.00
64: 6I-P2	−8.49	0.00	0.00

Table A9. Cases studied in Figure 13 (increments of radial displacements in mm).

	1.2U*(b)	1.2U*(c)	1.2U*(d)	1.2U*(e)
Level (m above sea level)	625	623	629.2	633
Opening (mm)	1.01	0.85	1.40	1.73
01: 0D crest	−0.20	−0.17	−0.28	−0.35
03: 0D-P0	−0.11	−0.09	−0.15	−0.19
05: 0D-P2	−0.39	−0.32	−0.54	−0.68
13: 1D-P0	−0.29	−0.23	−0.39	−0.49
15: 1D-P2	−0.16	−0.14	−0.22	−0.26
20: 2I crest	−0.28	−0.23	−0.39	−0.49
22: 2I-P0	−0.20	−0.17	−0.27	−0.35
24: 2I-P2	−0.11	−0.09	−0.15	−0.19
21: 2D crest	−0.12	−0.10	−0.17	−0.21
23: 2D-P0	−0.12	−0.10	−0.16	−0.21
25: 2D-P2	−0.07	−0.06	−0.09	−0.12
40: 4I crest	0.02	0.02	0.02	0.03
42: 4I-P0	0.01	0.01	0.02	0.01
44: 4I-P2	−0.02	−0.01	−0.02	−0.03
41: 4D crest	0.10	0.08	0.14	0.17
43: 4D-P0	0.09	0.07	0.12	0.15
45: 4D-P2	0.01	0.01	0.01	0.02
62: 6I-P0	0.12	0.10	0.16	0.20
64: 6I-P2	0.03	0.02	0.03	0.04
61: 6D crest	0.09	0.07	0.11	0.14
65: 6D-P2	0.02	0.02	0.03	0.04

Table A10. New cases studied in Figures 14–16 (increments of radial displacements in mm).

	1.1U*(b)	1.1U*(c)	1.1U*(d)
Level (m above sea level)	625	623	629.2
Opening (mm)	0.91	0.75	1.20
01: 0D crest	−0.13	−0.11	−0.18
03: 0D-P0	−0.07	−0.06	−0.09
05: 0D-P2	−0.15	−0.12	−0.21
13: 1D-P0	−0.11	−0.09	−0.15
15: 1D-P2	−0.06	−0.05	−0.08
20: 2I crest	−0.07	−0.06	−0.09
22: 2I-P0	−0.05	−0.04	−0.06
24: 2I-P2	−0.03	−0.02	−0.04
21: 2D crest	0.01	0.01	0.01
23: 2D-P0	−0.01	−0.01	−0.01
25: 2D-P2	−0.01	−0.01	−0.01
40: 4I crest	0.05	0.05	0.07
42: 4I-P0	0.04	0.03	0.06
44: 4I-P2	0.01	0.00	0.01
41: 4D crest	0.07	0.06	0.10
43: 4D-P0	0.06	0.05	0.09

References

1. Li, Z. Global Sensitivity Analysis of the Static Performance of Concrete Gravity Dam from the Viewpoint of Structural Health Monitoring. *Arch. Comput. Methods Eng.* **2021**, *28*, 1611–1646. [CrossRef]
2. ASCE Report Card for America's Infrastructure. 2021. Available online: https://ec.europa.eu/newsroom/cipr/redirection/document/79898 (accessed on 20 January 2025).

3. ICOLD EUROPEAN CLUB Dam Legislation. Working Group on Dam Legislation, FINAL REPORT. 2020. Available online: https://albcold.gov.al/wp-content/uploads/2021/03/ICOLD_EurClub-Dam_Legislation_Report-2020.pdf (accessed on 20 January 2025).
4. Wei, P.; Lin, P.; Peng, H.; Yang, Z.; Qiao, Y. Analysis of Cracking Mechanism of Concrete Galleries in a Super High Arch Dam. *Eng. Struct.* **2021**, *248*, 113227. [CrossRef]
5. Haftani, M.; Gheshmipour, A.A.; Mehinrad, A.; Binazadeh, K. Geotechnical Characteristics of Bakhtiary Dam Site, SW Iran: The Highest Double-Curvature Dam in the World. *Bull. Eng. Geol. Environ.* **2014**, *73*, 479–492. [CrossRef]
6. Novak, P.; Moffat, A.I.B.; Nalluri, C.; Narayanan, R. *Hydraulic Structures*, 4th ed.; CRC Press: Boca Raton, FL, USA, 2014; ISBN 9781315274898.
7. Ren, Q.; Xu, L.; Wan, Y. Research Advance in Safety Analysis Methods for High Concrete Dam. *Sci. China Ser. E Technol. Sci.* **2007**, *50*, 62–78. [CrossRef]
8. Jonker, M.; Espandar, R. Evaluation of Existing Arch Dam Design Criteria in Lieu of ANCOLD Guidelines. In Proceedings of the ANCOLD Conference, Gold Coast, Australia, 12–16 November 2008.
9. Pardo-Bosch, F.; Aguado, A. Damage Diagnosis in Concrete Dams with Presented Expansive Damage Based on Medical Propaedeutics. *J. Perform. Constr. Facil.* **2017**, *31*, 04017048. [CrossRef]
10. Abdulrazeg, A.A.; Noorzaei, J.; Jaafar, M.S.; Khanehzaei, P.; Mohamed, T.A. Thermal and Structural Analysis of Rcc Double-Curvature Arch Dam. *J. Civ. Eng. Manag.* **2014**, *20*, 434–455. [CrossRef]
11. Fu, S.; He, T.; Wang, G.; Zhang, S.; Zou, L.; Chen, S. Evaluation of Cracking Potential for Concrete Arch Dam Based on Simulation Feedback Analysis. *Sci. China Technol. Sci.* **2011**, *54*, 565–572. [CrossRef]
12. Lin, P.; Zhou, W.; Liu, H. Experimental Study on Cracking, Reinforcement, and Overall Stability of the Xiaowan Super-High Arch Dam. *Rock. Mech. Rock. Eng.* **2015**, *48*, 819–841. [CrossRef]
13. Sheibany, F.; Ghaemian, M. Effects of Environmental Action on Thermal Stress Analysis of Karaj Concrete Arch Dam. *J. Eng. Mech.* **2006**, *132*, 532–544. [CrossRef]
14. Fanelli, M. *Automated Observation for the Safety Control of Dams*; ICOLD Bulletin; International Commission on Large Dams: Paris, France, 1982; Volume 41.
15. Staiger, R. Recommended Procedures for Routine Checks of Electro-Optical Distance Meters. *Int. Fed. Surv. (FIG)* **2007**, *6*.
16. *ICOLD Dam Surveillance Guide*; Bulletin 158; International Commission on Large Dams: Paris, France, 2018.
17. Chrzanowski, A.; Szostak-Chrzanowski, A.; Steeves, R. Reliability and Efficiency of Dam Deformation Monitoring Schemes. In Proceedings of the CANADIAN DAM ASSOCIATION 2011 Annual Conference, Fredericton, NB, Canada, 15 October 2011.
18. Sharma, R.P.; PerezSaiz, M.A.; Pujol, A.; Melbinger, R.; Lampa, J.; Moore, D.; Poupart, M.; Bonaldi, P.; Shibata, I.; Mori, Y.; et al. *Automated Dam Monitoring Systems: Guidelines and Case Histories*; ICOLD: Paris, France, 2000.
19. Alba, M.; Fregonese, L.; Prandi, F.; Scaioni, M.; Valgoi, P. Structural Monitoring of a Large Dam by Terrestrial Laser Scanning. In Proceedings of the ISPRS Commission V Symposium, Dresden, Germany, 25–27 September 2006; pp. 1–6.
20. de Luis, J. Contraste En La Ejecución de Auscultaciones Geodésicas Por Métodos Clásicos y Con Láser Escáner. Ph.D. Thesis, University of Cantabria, Cantabria, Spain, 2009.
21. Ramos-Alcázar, L.; Marchamalo-Sacristán, M.; Martínez-Marín, R. Comparing Dam Movements Obtained with Terrestrial Laser Scanner (TLS) Data against Direct Pendulums Records. *Rev. Fac. Ing. Univ. Antioq.* **2015**, *76*, 99–106. [CrossRef]
22. Rüeger, J. Overview of Geodetic Deformations Measurements of Dams. In Proceedings of the Australian National Committee on Large Dams Conference (ANCOLD), Sydney, Australia, 19–22 November 2006; pp. 1–34.
23. Schneider, D. Terrestrial Laser Scanning for Area Based Deformation Analysis of Towers and Water Damns. In Proceedings of the 3rd IAG/12th FIG Symposium, Baden, Austria, 22–24 May 2006; pp. 22–24.
24. *SDL1x Operator's Manual*; Sokkia Topcon Co., Ltd.: Astugi, Japan, 2009.
25. Huggenberger AG. Coordiscope KK84. Available online: https://www.huggenberger.com/products/pendulum-measuring-system/coordiscope-kk84/ (accessed on 11 June 2024).
26. Product Catalogue Manufacturing Excellence 2018. Available online: https://www.soilinstruments.com/wp-content/uploads/2018/10/Soil-Instruments-Product-Catalogue-260718-min.pdf (accessed on 20 January 2025).
27. Siguel Gemin, A.R.; Santos Matos, É.; Faggion, P.L. Determination of Vertical Deviations of Guide Rails with Different Surveying Techniques. *Rev. Bras. Geomática* **2019**, *7*, 186. [CrossRef]
28. *TELELOT VDD2V4 Manual*; Huggenberger AG: Horgen, Switzerland, 2007.
29. *Geotechnical & Structural Instrumentation Product Catalog*; ROCTEST: Saint-Lambert, QC, Canada, 2017. Available online: https://smartec.ch/wp-content/uploads/2017/01/ROCTEST-CATALOG-EN.pdf (accessed on 20 January 2025).
30. *Leica AT930/AT960 User Manual*; Leica Geosystems AG: Heerbrugg, Switzerland, 2015.
31. Braun, J.; Dvořáček, F.; Štroner, M.; Urban, R. Testing Electronic Distance Meters on Short Absolute Laboratory Baseline. In Proceedings of the International Multidisciplinary Scientific GeoConference Surveying Geology and Mining Ecology Management, SGEM, Albena, Bulgaria, 17–26 June 2014.

32. Bryś, H.; Ćmielewski, K.; Gołuch, P.; Kowalski, K. The System of Automatic Laser Plumb-Line for Monitoring a Heavy Dam Wall. *Rep. Geod.* **2011**, *1/90*, 41–49.
33. Campos, A.; López, C.M.; Blanco, A.; Aguado, A. Structural Diagnosis of a Concrete Dam with Cracking and High Nonrecoverable Displacements. *J. Perform. Constr. Facil.* **2016**, *30*, 04016021. [CrossRef]
34. Blanco, A.; Cavalaro, S.H.P.; Segura, I.; Segura-Castillo, L.; Aguado, A. Expansions with Different Origins in a Concrete Dam with Bridge over Spillway. *Constr. Build. Mater.* **2018**, *163*, 861–874. [CrossRef]
35. Campos, A.; López, C.M.; Blanco, A.; Aguado, A. Effects of an Internal Sulfate Attack and an Alkali-Aggregate Reaction in a Concrete Dam. *Constr. Build. Mater.* **2018**, *166*, 668–683. [CrossRef]
36. Linsbauer, H.N.; Ingraffea, A.R.; Rossmanith, H.P.; Wawrzynek, P.A. Simulation of Cracking in Large Arch Dam: Part II. *J. Struct. Eng*. **1989**, *115*, 1616–1630. [CrossRef]
37. Leitão, N.S.; Castilho, E. Chemo-Thermo-Mechanical FEA as a Support Tool for Damage Diagnostic of a Cracked Concrete Arch Dam: A Case Study. *Eng* **2023**, *4*, 1265–1289. [CrossRef]
38. Oliveira, S.; Faria, R. Numerical Simulation of Collapse Scenarios in Reduced Scale Tests of Arch Dams. *Eng. Struct.* **2006**, *28*, 1430–1439. [CrossRef]
39. Wang, W.; Ding, J.; Wang, G.; Zou, L.; Chen, S. Stability Analysis of the Temperature Cracks in Xiaowan Arch Dam. *Sci. China Technol. Sci.* **2011**, *54*, 547–555. [CrossRef]
40. Zheng, D.; Huo, Z.; Li, B. Arch-Dam Crack Deformation Monitoring Hybrid Model Based on XFEM. *Sci. China Technol. Sci.* **2011**, *54*, 2611–2617. [CrossRef]
41. Zhuang, D.; Ma, K.; Tang, C.; Cui, X.; Yang, G. Study on Crack Formation and Propagation in the Galleries of the Dagangshan High Arch Dam in Southwest China Based on Microseismic Monitoring and Numerical Simulation. *Int. J. Rock Mech. Min. Sci.* **2019**, *115*, 157–172. [CrossRef]
42. Luo, D.; Lin, P.; Li, Q.; Zheng, D.; Liu, H. Effect of the Impounding Process on the Overall Stability of a High Arch Dam: A Case Study of the Xiluodu Dam, China. *Arab. J. Geosci.* **2015**, *8*, 9023–9041. [CrossRef]
43. Zhang, C.; Xu, Y.; Wang, G.; Jin, F. Non-Linear Seismic Response of Arch Dams with Contraction Joint Opening and Joint Reinforcements. *Earthq. Eng. Struct. Dyn.* **2000**, *29*, 1547–1566. [CrossRef]
44. Conde, A.; Salete, E.; Toledo, M.Á. Numerical Modeling of Cracked Arch Dams. Effect of Open Joints during the Construction Phase. *Infrastructures* **2024**, *9*, 48. [CrossRef]
45. *Academic Research Mechanical 2022*; Ansys Inc.: Canonsburg, PA, USA, 2022.
46. *Concrete Masonry Handbook*; Portland Cement Association: Chicago, IL, USA, 1951.
47. *PCI Design Handbook*; Helmuth Wilden, P.E., Ed.; Precast/Prestressed Concrete Institute: Chicago, IL, USA, 1971.
48. Conde, A.; Toledo, M.Á.; Salete, E. Cracks in Arch Dams: An Overview of Documented Instances. *Appl. Sci.* **2024**, *14*, 7580. [CrossRef]